Met. Mater. Int., Vol. 22, No. 3 (2016), pp. 519~526
doi: 10.1007/s12540-016-5595-7

Microstructure and Texture Evolution of AA 6063 During an Ex-ECAE Process

Cheng-Hsien Liu, Hsin-Chih Lin*, and Yu-Tung Hsu

Department of Materials Science and Engineering, National Taiwan University,
1, Roosevelt Road, Sec. 4, Taipei, 10617 Taiwan

(received date: 30 October 2015 / accepted date: 28 December 2015)

Equal channel angular extrusion (ECAE) has been studied at the lab scale for many years. However, few successful industrial applications of the ECAE process have been reported. In the present work, a process referred to as Ex-ECAE that was composed of two processes of the direct extrusion and the ECAE via route C, was developed. The Ex-ECAE process was developed to refine the microstructure of the extrudate, particular the coarse grain layer (CGL) on the surface of the extrudate. The Ex-ECAE die with a die angle of 120° contained three segments and was used in the conventional direct extrusion press. The high friction and the continuous routes of the ECAE resulted in asymmetric dead metal zones (DMZs) to be formed at the corners of the die channel. It revealed that the visible grains in the CGL were refined and became invisible due to the intense shear deformation as the CGL flowed along the boundaries of the asymmetric DMZs. The textures of the Ex-ECAE at the various segments were studied by EBSD. This study demonstrated that the ECAE process could be scaled up using the extrusion press. Success or lack of success depended on the capacity of the extrusion press and the die design.

Keywords: extrusion, texture, recrystallization, grain growth, grain refinement

1. INTRODUCTION

Equal channel angular extrusion (ECAE) has been studied at the lab scale for many years [1-14]. As shown in Fig. 1(a), the die of an ECAE is quite simple. It contains two channels of equal cross section that meet at a die angle Φ. The lubricated rod billet is pressed through the channels. Under ideal conditions, the majority of the billet is deformed in a narrow deformation zone at the plane of intersection of the two channels. On the intersected plane (the shear plane), a simple shear is imposed on the rod billet [1-2]. The dimensions of the cross section are almost unchanged during the ECAE process. Therefore, the deformed rod billet can be reinserted into the die to impose more plastic strain. The ECAE process became well known as an effective technique for grain refinement of a bulk material [9-10,15].

However, although the ECAE process has been studied at the lab scale for many years, few successful industrial applications of the ECAE process have been reported [16-18]. Moreover, the extrudate of the ECAE process was usually a raw material, for example, forging stock, but not a product or a semi-product. The length of the rod billet used and the extrudate were short because of the inlet channel is short. The profile of the cross section of the rod billet was usually quite simple. For a product with a complex or irregular cross-sectional profile, the manufacture of the initial rod billet might be very difficult. Moreover, the ECAE is not a continuous process. This is disadvantageous in terms of production efficiency. However, these drawbacks of the ECAE described above can be improved by combining this process with the direct extrusion process.

In the direct extrusion process, a preheated billet was placed in a heated container, and a stem or ram protected by a dummy block then pressed the billet through the die with an opening in the shape of the desired profile. The deforming billet in the container was divided into three main regions: a primary deformation zone, a dead metal zone (DMZ) and an intense shear deformation zone [18-20]. The materials that flowed through the shear deformation zone would have a large shear strain and a high temperature. Therefore, dynamic recrystallization will occur in the shear deformation zone. Then, these intense shear deformed materials will create a "visible" coarse grain layer (CGL) on the surface of the extrudate [21-26]. The extrudate with the CGL is typically regarded as an undesirable product and must be scrapped. CGL could cause many problems, such as bending failure, orange peel finish, streaking and variations in surface brightness [21]. Typically,

*Corresponding author: hclinntu@ntu.edu.tw

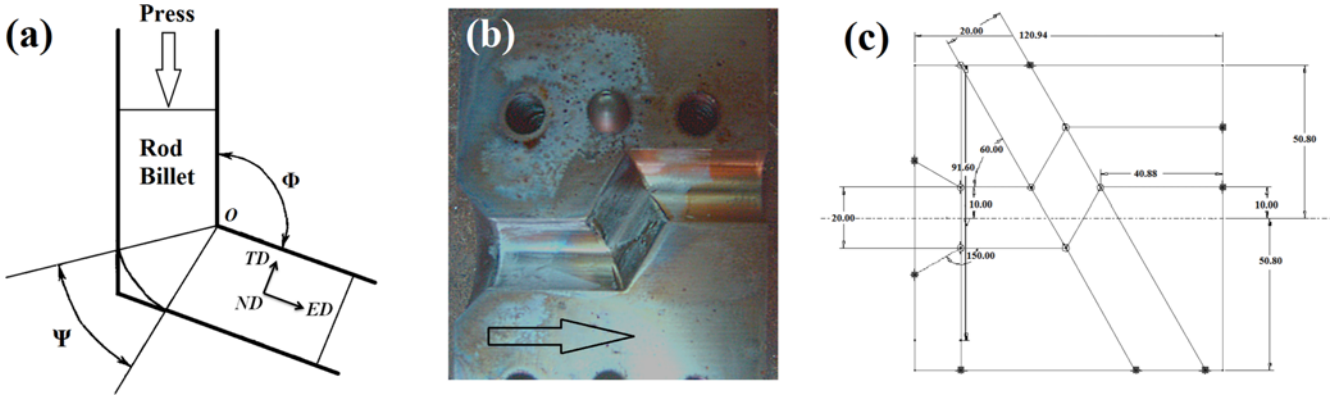

Fig. 1. (a) Schematic drawing of the ECAE process. (b) one half of the designed Ex-ECAE die used in the present study. Diameter of the channel was 20 mm. Extrusion direction is indicated by the black hollow arrow. (c) schematic drawing of the designed Ex-ECAE die.

the CGL was removed by machining or refined by thermo-mechanical treatment (TMT). However, these methods result in reduced productivity and increased costs.

In this study a process, referred to as the Ex-ECAE process, which was composed of the direct extrusion and the ECAE via route C two processes, was developed. The Ex-ECAE die, as shown in Fig. 1(b) and 1(c), with a die angle of 120° contained three segments and was used in the conventional direct extrusion press. Considering the capacity of the existed direct extrusion press, Ex-ECAE die was designed with a high die angle and with only two passes of the ECAE process. However, the refinement efficiency was increased as the die angle was decreased and the pass number was increased. The first segment of the Ex-ECAE (i.e., direct extrusion segment) could continuously produce long rod billets with any cross-sectional profile. Therefore, using the billet-to-billet loading method, the Ex-ECAE process could be regarded as a continuous process. The second and third segments (ECAE segment) were designed to refine the microstructure of the rod billet, particular the CGL (coarse grain layer) on the surface layer of the extrudate.

Finally, it is well known that a heavily deformed material usually contains a strong texture. However, texture is not a desired phenomenon for most structural material applications. Therefore, it is quite important to understand the texture of the product for structural applications. In the present study, the textures of the Ex-ECAE sample at various segments are measured using EBSD.

2. EXPERIMENTAL PROCEDURES

A DC (direct-chill) cast AA 6063 billet with a diameter of 88.9 mm was homogenized at 470 °C for 8 h. After homogenization, a 250 mm long billet was cut and preheated to 250 °C. In the direct extrusion process, the temperatures of the Ex-ECAE die and the container were both set at 200 °C. The ram speed was fixed at 1.5 mm/s. The diameter of the extrudate (i.e., rod billet) was 20 mm. The speed of the rod billet flow through the channel of the die was approximately 30 mm/s. After the Ex-ECAE process was finished, the material left in the channel, which was referred as to Ex-ECAE sample, was cooled down to room temperature in the die. Then, the Ex-ECAE sample was cut along the parting line. After polishing, the parting plane of the Ex-ECAE sample was immersed in a 10% NaOH solution for 20 min at room temperature to reveal the macrostructure and the flow pattern of the material. To compare the different effects between the Ex-ECAE and ECAE processes, a 50 mm long annealed bar with 20 mm diameter of AA 6063 without lubrication was put inside the die channel of the first segment in advance. During the Ex-ECAE process, the annealed bar was pressed through the ECAE segment by the Ex-ECAE extrudate. The annealed rod that flowed through the ECAE segment only was referred to ECAE sample. The ECAE sample was short and was totally out of the die, rather than was taken from the die channel.

To measure the textures, the EBSD specimens were sampled from the core of the billet, and the core and sub-surface of the Ex-ECAE sample at various segments in the transverse cross section. The EBSD specimens were twin-jet polished in a 30% HNO_3 + 70% CH_3OH solution at -30 °C and at 20 V. The EBSD and CPF (Continuous Pole Figure) analyses were carried out by using a system of NOVA NANO SEM 450 + EDAX/EBSD. However, in the present study the texture is indexed in the form - plane of the transverse cross section of the sample/direction of the normal of the die's parting plane.

3. RESULTS AND DISCUSSION

3.1. The Analysis of the AA 6063 Billet

Figure 2 shows the grain structure of the DC cast AA 6063 billet used in the present study. During the DC casting, the Al-Ti-B wire is added to the melt for grain refinement [27]. The use of the grain refiner results in the growth direction of the nuclei is not influenced by the heat flow. Therefore, the

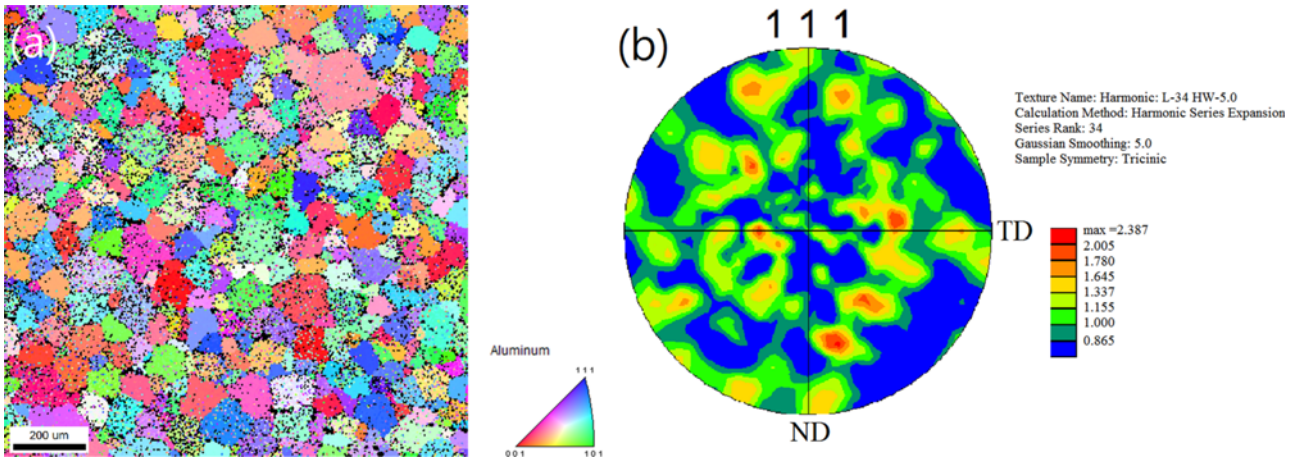

Fig. 2. (a) EBSD image of the grain structure of the extrusion billet AA 6063 used in the present study. (b) the CPF of the AA 6063 extrusion billet.

billet contains equiaxed grains, as shown in Fig. 2(a). The grain size of the billet is approximate 200 μm. As expected that the billet with the equiaxed grain structure has a random texture, as shown in Fig. 2(b).

3.2. Macrostructures and Flow Patterns of the Extrusion, Ex-ECAE and ECAE Processes

Figure 3 and Fig. 4 show the macrostructures and flow patterns of the Ex-ECAE and ECAE process, respectively. In reality, the first segment of the Ex-ECAE process is only subjected to an extrusion process. Therefore, the macrostructure of the first segment represents the one of the extrusion process.

In Fig. 3, the first segment of Ex-ECAE sample shows a typical macrostructure of the direct extrusion, i.e., a fibrous structure covered with a visible recrystallized CGL on the surface of the extrudate. The grain sizes of the CGL are approximate 0.68 mm - 2 mm. The large plastic strain (extrusion plastic strain is 2.932) deformation results in the development of the fibrous microstructure in the core region, which are aligned parallel to the extrusion direction. As shown in Fig. 3, the CGL with visible equiaxed grains in the first segment become more longitudinal when it flows through the second segment. However, the CGL is thinned during it flows through

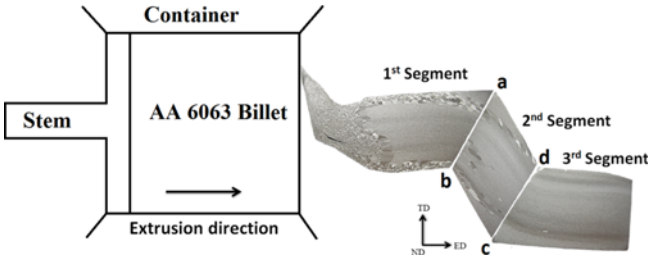

Fig. 3. The macrostructure and flow pattern of the Ex-ECAE sample at various segments. A sketch of the direct extrusion process was also shown in the left.

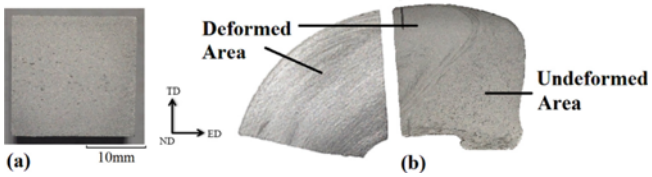

Fig. 4. The macrostructure and flow pattern of (a) the annealed rod billet and (b) the ECAE sample.

the die channel. Finally, the CGL disappeared before it enters the third segment. In the final stage, the grains at the whole cross section of the Ex-ECAE sample are invisible.

In terms of the ECAE process, an annealed rod containing larger grain size (~200 μm) at the core, as shown in Fig. 4(a), is chosen to evaluate the grain refinement of the ECAE process. Figure 4(b) shows the macrostructure and flow pattern of the ECAE sample. The ECAE sample is not straight due to the non-uniform flow in the die channel. It is obviously that the grains at the whole section of the ECAE sample are invisible. From Fig. 3 and Fig. 4, it may conclude here that regardless of the coarse grains are, the ECAE segment in the Ex-ECAE die without any lubrication can refine them to the extent invisible. However, ECAE sample has an undeformed area as shown in Fig. 4(b). It means that the ECAE process has less productivity than Ex-ECAE process.

3.3. Refinement of the Coarse Grain Layer on the Surface of the Ex-ECAE sample

Figure 5 shows the grain structures of the surface of the Ex-ECAE sample at various segments. It can be seen in Fig. 5 that the grains of the CGL on the surface are refined during the Ex-ECAE process. At the first segment, the CGL contains coarse equiaxed grains. These coarse equiaxed grains become longitudinal as they flow into the second segment. At the third segment, the coarse equiaxed grains of the CGL are refined to fine equiaxed grains. In fact, at the second segment, the

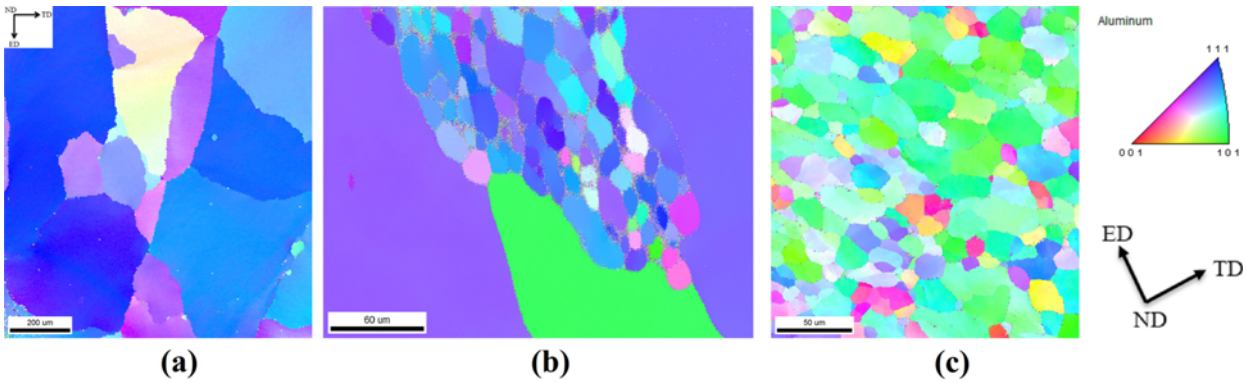

Fig. 5. The grain structures of the surface of the Ex-ECAE sample at various segments. (a) the first segment, (b) the second segment, and (c) the third segment.

grain structure is a mixture of the majority of longitudinal grains and some recrystallized fine grains.

In the ECAE process, the rod billets are usually well lubricated. However, in the Ex-ECAE process, the rod billet is produced at the first segment and not to be lubricated. Moreover, the continuous routes of the designed ECAE resulted in a back pressure effect [4]. These two factors led to the formation of the DMZs, as shown in Fig. 3, at the outside corners (a and c) and the inner corners (b and d), respectively. However, it is interesting that the DMZs that occurred at the corners are asymmetric. The asymmetric flow pattern results from the corners, for example, a and b, are too close and the high friction of the die channel. To obey the continuum conditions between the DMZ and CGL, the CGL would be subject to a high intense shear stress when it flowed through these DMZ boundaries. The intensity of the shear strain is high and caused a color difference between the refined CGL and the core materials, as shown in Fig. 3 in the third segment. Accordingly, the grain subdivision mechanism, a metal under heavily cold plastic deformation could be subdivided by grain boundaries and dislocation boundaries that formed during plastic deformation [28-31]. An EBSD specimen is sampled from the CGL near the DMZ b, as shown in Fig. 3, to observe the subdivision of the coarse grains. The subdivision of the coarse grain with a diameter of 0.68 mm - 2 mm in the CGL is demonstrated in Fig. 6. The flow direction of the CGL is indicated by a white arrow. Figure 6 showed that one of the longitudinal coarse grains in the CGL is subdivided into small equiaxed grains. These continuous dynamic recrystallized grains had a diameter of 15.5-25.8 μm. The original grain boundary profile could still be identified. Up to 86% of these recrystallized grains are bounded by HAGBs (high angle grain boundaries).

3.4. Refinement of the Core Materials of Ex-ECAE sample

The evolutions of the grain structure of core materials of the Ex-ECAE sample at various segments are shown in Fig. 7. It reveals that the huge longitudinal grains are refined and become an equiaxed grain structure at the second and the third segments, as shown in Fig. 7(b) and 5(c), respectively. The grain boundaries of the huge longitudinal grains at the first segment are characterized by their serrated and there existed many embellished small equiaxed grains, as shown in Fig. 7(a). These characteristics indicated the occurrence of so-called GDRX (geometric dynamic recrystallization) [32-36]. GDRX usually occurs when the materials are deformed with large plastic strains at an elevated temperature, such as during the extrusion process. During plastic deformation, the original grains became highly elongated and the grain boundaries would migrate along subgrain boundaries and became serrated. When the thickness of these elongated grains is reduced to approximately two subgrain diameters, some serrations met causing the grains to pinch off, and new equiaxed grains

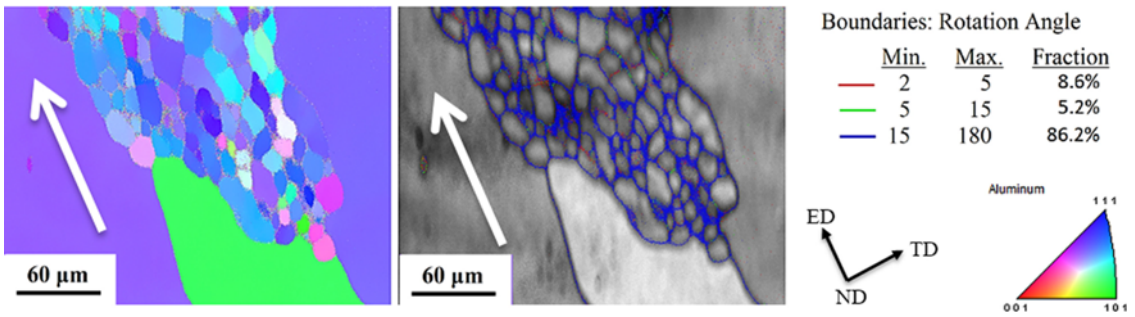

Fig. 6. Representation of the grain subdivision that occurred in a coarse grain of the coarse grain layer.

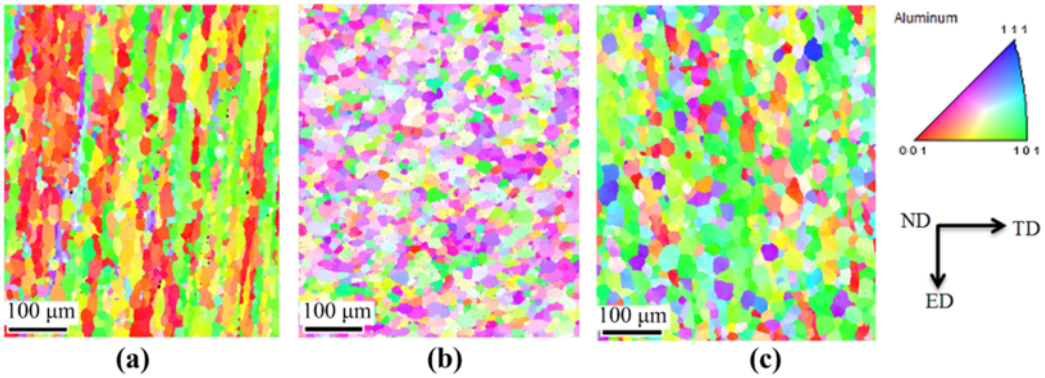

Fig. 7. The grain structures of the core of the Ex-ECAE sample at various segments. (a) the first segment, (b) the second segment, and (c) the third segment.

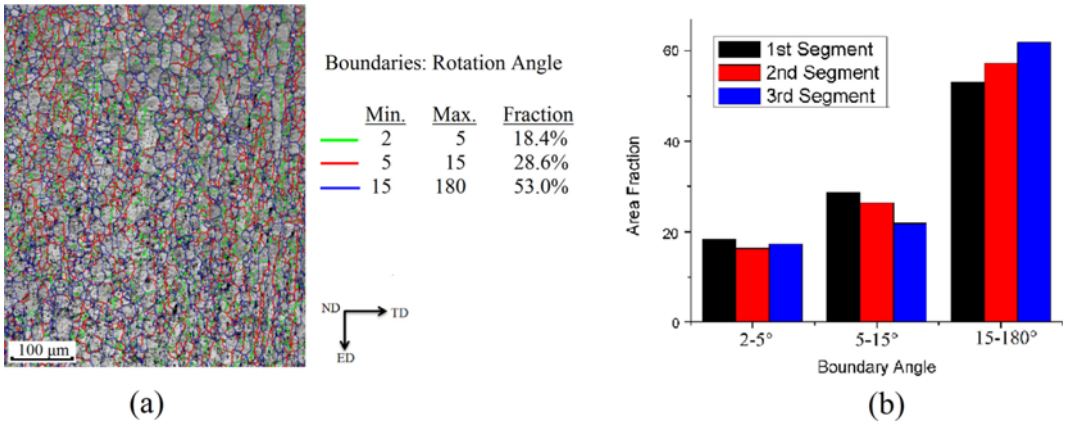

Fig. 8. (a) The grain boundary misorientation angle distribution of the core of the Ex-ECAE sample at the first segment. color-coding showed the spatial location of selected misorientation ranges. (b) the grain boundary angle distribution of the core of the Ex-ECAE sample at various segments.

are created [36]. Figure 8 illustrated the variation of grain boundary angles at the various segments. The Ex-ECAE sample at the first segment, as shown in Fig. 8(a), contained a higher fraction of LAGB (low angle grain boundaries). As shown in Fig. 8(a), the fraction of LAGB is up to 47%. However, as the material flows into the second and the third segment (ECAE segment), these LAGBs will be transferred to HAGBs. As shown in Fig. 8(b), as the Ex-ECAE process progress, more and more HAGBs. In the second segment, the subdivided fine equiaxed subgrain has a grain size of approximately 25 μm, as shown in Fig. 7(b). However, these subgrains slightly grow to a grain size of approximately 30 μm when they flow through the third segment. Subgrain growth has been attributed to either one of two distinctly different mechanisms: (a) subgrain coalescence [37-39] or (b) migration of sub-boundaries [40-41].

3.5. Texture Evolution of the Ex-ECAE Sample

The CPF of the core of the Ex-ECAE sample at various segments are shown in Fig. 9. The texture indices of this study are summarized in Table 1. The CPF of the first segment of the

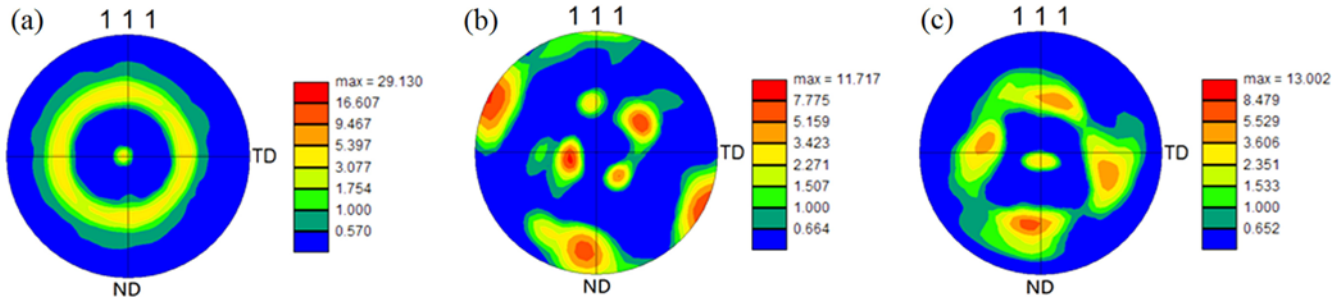

Fig. 9. The continuous pole figures of the core of the Ex-ECAE sample at various segments. (a) the first segment, (b) the second segment, and (c) the third segment.

Table 1. Summarization of the texture indices of the Ex-ECAE samples at various segment

Sample	Euler angle (φ_1, Φ, φ_2)	Texture Indices
C-1	fiber texture	<0 0 1> Strong
	fiber texture	<1 1 1> Weak
C-2	(26, 79.8, 50)	{1 1 0} <1 -2 1> 48.6x
	(9.4, 32.6, 15)	{0 1 1} <2 -1 0> 21.0x
C-2	(76.2, 6, 50)	{0 0 1} <-1 -1 0> 25.4x
	(5.4, 54.8, 35)	{1 1 1} <1 -1 0> 8.90x
S-1	(20.1, 51, 35)	{1 1 1} <1 -1 0> 113.7x
	(47.2, 44.5, 30)	{1 2 2} <1 -2 1> 49.9x
S-2	(0, 69.5, 55)	{4 3 2} <1 -1 0> 17.5x
	(57.5, 55.3, 15)	{0 1 1} <4 6 7> 8.20x
S-2	(48.8, 77.5, 40)	{1 1 0} <1 -1 2> 18.2x
	(72.7, 36.3, 75)	{1 0 1} <-1 -1 1> 18.0x

C: core. S: surface. 1, 2 and 3: the first, second and third segment, respectively.

core has a zone with a uniform band, as shown in Fig. 9(a). As expected, the first segment of the core exhibits a perfect fiber texture, due to the axisymmetric deformation mode of the extrusion process. The texture of the first segment consists of the expected mixture of strong <0 0 1> and weak <1 1 1> fiber components. This is a typical fiber texture often occurs in the wire drawing process of FCC metals and alloys [42]. However, the center of the zone does not coincide with the center of the pole figure. This phenomenon shall result from the processing of the specimen preparation. As the first segment of the core flows into the second segment, the deformation mode changes from axisymmetric deformation mode to simple shear deformation mode. In the second segment, simple shear occurring on the shear plane will destroy the fiber texture and create a new texture. As shown in Fig. 9(b), the second segment has a texture of strong {1 1 0} <1 -2 1> + weak {0 1 1} <2 -1 0>. However, the texture of the main component is the well-known "alloy" or "brass" type texture [42]. The texture of the third segment, as shown in Fig. 9(c), is also a mixture of two components - the strong component {0 0 1} <-1 -1 0> and the weak component {1 1 1} <1 -1 0>. However, the CPF of Fig. 9(c) shows that an incomplete zone is developed. Iwahashi *et al*. [43] has illustrated that each ECAE process had its own particular shearing pattern. The ECAE via route C is a reverse process because the shear stress is reversed on the same shear plane between the passes. It implies that the texture of the second segment will be reversed to that of the first segment as it flows into the third segment. However, the deformation modes between the direct extrusion (the first segment) and ECAE (the second and the third segments) are quite different. The fiber texture is difficult to be completely recovered in the third segment. In the present study, there are only two passes of ECAE in the Ex-ECAE die. It is expected that the more passes the Ex-ECAE die had, the less recovery of the fiber texture would be.

The textures of the surface at various segments are shown in Fig. 10. Comparing of Fig. 9(a) and Fig. 10(a), the texture difference between the core and the surface of the first segment is enormous. At the first segment, the texture of the surface material consists of the mixture of strong {1 1 1} <1 -1 0> and weak {1 2 2} <1 -2 1>. It is believed that the dynamic recrystallization results in the formation of the CGL and destroys the original deformed texture of the surface during the extrusion. As the surface material flows into the second segment, the texture transfers to the mixture of strong {4 3 2} <1 -1 0> + weak {0 1 1} <4 -6 7>, as shown in Fig. 10(b). It is interesting to note that as the surface material flows into the third segment, two incomplete zones appear, as shown in Fig. 10(c). One is located at the center and the other is located at the circumference of the CPF. It reveals that an incomplete fiber texture has been developed in the surface material during Ex-ECAE process. In terms of surface material, the deformed texture, which is developed during the ECAE process, is mainly strongly dependent on the friction shear stress rather than the simple shear stress. As the Ex-ECAE sample flows through the die channel, it is subjected to an annular shear stress resulted from the friction on the surface. Then a shear stress gradient, also a velocity gradient, will be built up along the radial of the sample. And the advancing cross section plane of the sample will be a curved surface rather than a flat plane. The flow speed of surface material will be slower than that of the core material. To obey the continuum theory, the surface material will subject to an intense shear deformation between the die channel wall and the core material. Under the intense shear deformation,

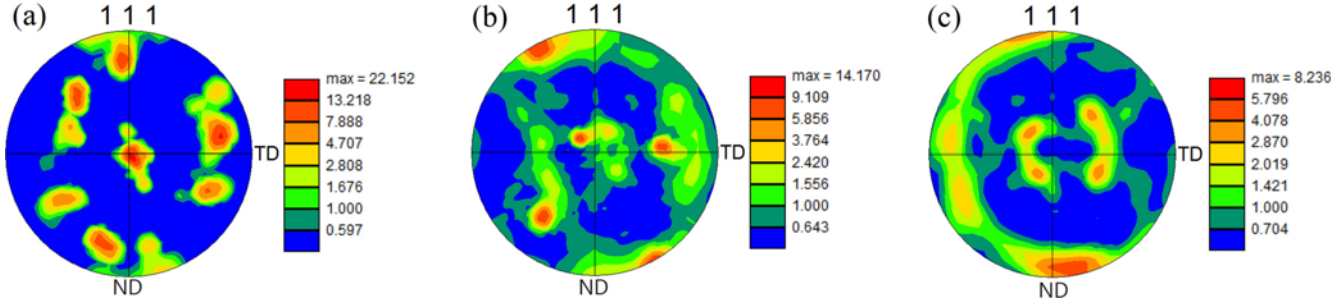

Fig. 10. The continuous pole figures of the surface of the parting line at various segments. (a) the first segment, (b) the second segment, and (c) the third segment.

a fiber texture will be developed in the surface material. Finally, in comparison of Fig. 9 and Fig. 10, there exists a texture gradient from the center to the surface along the radial of the Ex-ECAE sample. It results from the strain gradient built along the radial of the sample during Ex-ECAE process, especially during the extrusion step.

3.6. The Comparison of the Ex-ECAE Process and the ECAE Process

The operating conditions of the Ex-ECAE process and ECAE process are quite different. (1) The rod billets used in the ECAE are short, lubricated and loaded piece-by-piece. The cross-sectional profiles of the rod billet are simple and regular. In the Ex-ECAE process, the rod billets are extruded from an extrusion billet. Therefore, a continuous, unlubricated and long rod billet can be supplied. Additionally, the rod billets with any complex and irregular cross-sectional profile can be directly extruded if the extrusion die can be designed and machined. (2) The initial microstructure of the ECAE rod billets is usually annealed, and the grains have a low dislocation density. However, the Ex-ECAE rod billet has fibrous structures and contains many subgrains with LAGBs and/or HAGBs. Therefore, with the help of extrusion, only one pass of the ECAE process is needed to refine the grains of the rod billets. (3) Unlike the ECAE, the rod billets used in the Ex-ECAE are produced without any lubrication. High friction and the continuous routes of the designed ECAE result in the formation of the asymmetric DMZs at the corners of the channel. The formation of the asymmetric DMZs resulted in the refinement of the CGL. (4) ECAE is a discontinuous process. However, using the billet-to-billet loading method [19], Ex-ECAE can be regarded as a continuous process. (5) The flow speed of the rod billet in the Ex-ECAE process, which depends on the extrusion ratio and the ram speed, is much faster than the flow speed in the ECAE process.

4. CONCLUSIONS

(1) An Ex-ECAE process composed of extrusion and ECAE via route C two processes is developed. The Ex-ECAE die with a die angle of 120° contained three segments and is used in a conventional direct extrusion press.

(2) The high friction and the continuous routes of the designed ECAE resulted in asymmetric DMZs to be formed at the corners of the channel. The study revealed that the visible grains in the CGL are refined and became invisible due to the shear deformation when the CGL flowed along the boundary of the asymmetric DMZs.

(3) Moreover, most of the huge longitudinal grain structures in the core of the Ex-ECAE sample could be refined and became equiaxed grains when the core flowed through the ECAE segment.

(4) The deformed textures of the Ex-ECAE at the various segments are studied. In the first segment, the texture of the extrudate is a typical fiber texture: strong <001> + weak <111>. The texture that resulted from the extrusion is an axisymmetric deformation process. In the second segment, a specific weaker deformed texture, strong {1 1 0} <1 -2 1> + weak {0 1 1} <2 -1 0>, is developed. In the third segment, the texture of the extrudate is reversed to an incomplete fiber texture: strong {0 1 1} <-1 -1 0> + weak {1 1 1} <1 -1 0>.

(5) This study demonstrated that the ECAE process could be scaled up using a conventional direct extrusion press. Success or lack of success depended on the capacity of the extrusion press and Ex-ECAE die design.

REFERENCES

1. V. M. Segal, *Mater. Sci. Eng. A* **197**, 157 (1995).
2. V. M. Segal, *Mater. Sci. Eng. A* **271**, 322 (1999).
3. R. Luri, C. J. Luis, D. Salcedo, J. León, J. P. Fuertes, and I. Puertas, *Procedia Engineering* **63**, 540 (2013).
4. J. R. Bowen, A. Gholinia, S. M. Roberts, and P. B. Prangnell, *Mater. Sci. Eng. A* **287**, 87 (2000).
5. I. Mazurina, T. Sakai, H. Miura, O. Sitdikov, and R. Kaibyshev, *Mater. Sci. Eng. A* **473**, 297 (2008).
6. I. Puertas, C. J. Luis-Pérez, D. Salcedo, J. León, R. Luri, and J. P. Fuertes, *Procedia CIRP* **12**, 288 (2013).
7. X. X. Wang, M. He, Z. Zhu, K. M. Xue, and P. Li, *T. Nonferr. Metal. Soc.* **25**, 2122 (2015).
8. Y. L. Duana, G. F. Xua, L. Tanga, Z. Lia, and G. Yang, *Mater. Sci. Eng. A* **648**, 252 (2015).
9. M. J. Zehetbauer and Y. T. Zhu, *Bulk Nanostructured Materials*, first ed., pp. 203-216, Wiley-VCH Verlag GmbH & Co., Weinheim (2009).
10. M. J. Zehetbauer and R. Z. Valiev, *Nanomaterials by Severe Plastic Deformation*, first ed., pp. 131-137, Wiley-VCH Verlag GmbH & Co., Weinheim (2002).
11. O. Sitdikov, E. Avtokratova, and T. Sakai, *J. Alloy. Compd.* **648**, 195 (2015).
12. I. Puertas, C. J. Luis Pérez, D. Salcedo, J. León, J. P. Fuertes, and R. Luri, *Mater. Design* **52**, 774 (2013).
13. A. Jäger, V. Gärtnerova, and K. Tesař, *Mater. Sci. Eng. A* **644**, 114 (2015).
14. I. J. Beyerlein and L. S. Tóth, *Prog. Mater. Sci.* **54**, 427 (2009).
15. R. Z. Valiev, R. K. Islamgaliev and I. V. Alexandrov, *Prog. Mater. Sci.* **45**, 103 (2000).
16. S. Ferrasse, F. Alford, S. Grabmeier, A. Düvel, R. Zedlitz, and S. Strothers, *ECAE® Targets with Sub-Micron Grain Structures Improve Sputtering Performance and Cost-of-Ownership*, https://www.researchgate.net/publication/267221044_ECAE_R_Targets_with_Sub-Micron_Grain_Structures_Improve_Sputtering_Performance_and_Cost-of-Ownership (accessed October 28, 2014).
17. R. Srinivasan, B. Cherukuri, and P. K. Chaudhury, *Mater. Sci. Forum* **503-504**, 371 (2006).

18. P. K. Chaudhury, B. Cherukuri, and R. Srinivasan, *Mater. Sci. Eng. A* **410-411**, 316 (2005).
19. M. Bauser, G. Sauer, and K. Siegert, *Extrusion*, second ed., pp. 9-48, ASM International®, Ohio (2006).
20. T. Sheppard and S. J. Paterson, *J. Mech. Work. Technol.* **7**, 39 (1982).
21. *Comalco (Rio Tinto Aluminium) Extrusion Guides for 6000 Series Alloys*, Coarse Grain Surface Layer in 6000 Series Extrusions, http://sales.riotintoaluminium.com/document_get.aspx?id=143.
22. M. Schikorra, L. Donate, L. Tomesani, and A. E. Tekkaya, *J. Mech. Work. Technol.* **21**, 1445 (2007).
23. W. H. Van Geertruyden, W. Z. Misiolek, and P. T. Wang, *J. Mater. Sci.* **40**, 3861 (2005).
24. W. Libura and J. Zasadzinski, *J. Mater. Process. Tech.* **34**, 517 (1992).
25. P. Kazanowski, H. M. Browne, W. Libura, and W. Z. Misiolek, *Mater. Sci. Eng. A* **404**, 235 (2005).
26. X. Duan and T. Sheppard, *Mater. Sci. Eng. A* **351**, 282 (2003).
27. J. Hirsch, *Arch. Metall. Mater.* **50**, 21 (2005).
28. Q. L. Zhao and B. Holmedal, *T. Nonferr. Metal. Soc.* **24**, 2072 (2014).
29. H. Zhao, S. Ni, M. Song, X. Xiong, X. Liang, and H. Li, *Mater. Sci. Eng. A* **645**, 328 (2015).
30. M. A. Kumara and S. Mahesh, *Int. J. Plasticity* **44**, 95 (2013).
31. D. A. Hughes and N. Hansen, *Acta Mater.* **45**, 3871 (1997).
32. L. Donati, A. Segatori, M. E. Mehtedi, and L. Tomesani, *Int. J. Plasticity* **46**, 70 (2013).
33. M. E. Kassner and S. R. Barrabes, *Mater. Sci. Eng. A* **410-411**, 152 (2005).
34. F. Montheillet, J. Lepinoux, D. Weygand, and E. Rauch, *Adv. Eng. Mater.* **3**, 587 (2001).
35. R. Kaibyshev, I. Mazurina, and O. Sitdikov, *Mater. Sci. Forum* **467-470**, 1199 (2004).
36. H. J. McQueen, S. Spigarelli, M. E. Kassner, and E. Evangelista, *Hot Deformation and Processing of Aluminum Alloys*, first ed., pp. 267-300, CRC Press, New York (2011).
37. Y. J. Li, A. Kostka, P. Choi, S. Goto, D. Ponge, R. Kirchheim, and D. Raabe, *Acta Mater.* **84**, 110 (2015).
38. R. D. Doherty and J. A. Szpunar, *Acta Metallurgica* **32**, 1789 (1984).
39. R. Sandstrom, *Acta Metallurgica* **25**, 897 (1977).
40. T. Furu, R. Orsund, and E. Nes, *Acta Metall. Mater.* **43**, 2209 (1995).
41. R. Sandstrom, *Acta Metallurgica* **25**, 905 (1977).
42. U. F. Kocks, C. N. Tomé, and H. R. Wenk, *Texture and Anisotropy: Preferred Orientations in Polycrystals and Their Effect on Materials Properties*, first ed., pp. 178-239, Cambridge University Press, England (1998).
43. Y. Iwahashi, Z. Horita, M. Nemoto, and T. G. Langdon, *Acta Mater.* **46**, 3317 (1998).